



# Studies of structural, microstructural, dielectric, and electrical characterization of BiNaZnMoO<sub>6</sub> double perovskite

Swati PANDA<sup>1</sup>, Supriya BARIK<sup>1</sup>, Ritu Purna SAHU<sup>1</sup>, Adwit Prasad SAHU<sup>1</sup>, S. MISHRA<sup>1</sup>, and S. K. PARIDA<sup>1,\*</sup>

<sup>1</sup> Department of Physics, ITER, Siksha 'O' Anusandhan Deemed to be University, Bhubaneswar-751030, India

\*Corresponding author e-mail: santoshparida@soa.ac.in

## Received date:

19 December 2024

## Revised date:

25 January 2025

## Accepted date:

2 March 2025

## Keywords:

BiNaZnMoO<sub>6</sub> ceramic;  
Orthorhombic crystal symmetry;  
SEM micrograph;  
Semiconducting nature;  
Thermally activated conduction mechanism

## Abstract

This study investigates the structural, microstructural, dielectric, and electrical properties of BiNaZnMoO<sub>6</sub> (BNZM) ceramic synthesized using a conventional solid-state reaction method. Preliminary structural analysis using X-ray diffraction (XRD) suggests orthorhombic crystal symmetry. Scanning electron microscopy (SEM) micrographs reveal a uniform distribution of well-grown grains with well-defined grain boundaries, which may contribute to the enhanced dielectric properties. Energy dispersive X-ray spectroscopy (EDX) analysis confirms the presence of all constituent elements Bi, Na, Zn, Mo, and O in the studied sample. Dielectric spectra analysis as a function of frequency and temperature indicates the formation of high-quality dielectric materials, evidenced by a high dielectric constant and low loss. Impedance spectroscopy supports the semiconducting nature of the sample. Modulus analysis reveals a non-Debye type of relaxation process. The study of AC conductivity suggests a thermally activated conduction mechanism. Furthermore, Cole-Cole and Nyquist plots confirm the semiconducting behavior, which is corroborated by resistance versus temperature analysis. These findings suggest potential applications in energy storage devices.

## 1. Introduction

Single perovskite ceramic materials are a class of compounds with the general formula ABX<sub>3</sub>, where **A** is a larger cation (typically an alkali, alkaline earth, or rare-earth element), **B** is a smaller cation (usually a transition metal), and **X** is an anion, most commonly oxygen. The perovskite structure is highly versatile, allowing for various substitutions at the A and B sites, which enables the tuning of a wide range of physical properties, such as ferroelectricity, piezoelectricity, and high dielectric constants. Due to these properties, perovskite materials are extensively used in applications like capacitors, sensors, and energy harvesting devices [1-7].

Double perovskite ceramics, with the general formula A<sub>2</sub>BB'X<sub>6</sub>, incorporate two distinct cations (B and B') in the B-site, resulting in a more complex structure that can enhance or modify the material's electrical, magnetic, and optical properties. This increased compositional flexibility enables the tuning of material properties for specific applications, such as multiferroics, catalysts, and thermoelectric materials. Compared to single perovskites, double perovskites often exhibit improved thermal stability, higher dielectric constants, and novel electronic behavior. Due to their unique structural and functional properties, double perovskites have garnered significant interest for diverse applications across various fields. One of their primary applications is in electronic devices, where double perovskites serve as high-performance dielectrics and capacitors, benefiting from their high dielectric constants and low losses. They are also utilized in multiferroic materials, which exhibit simultaneous ferroelectric and magnetic properties, making them suitable for advanced data storage

and spintronic devices. In catalysis, double perovskites are employed for various chemical reactions, including oxygen evolution in fuel cells and photocatalysis for water splitting [8,9]. Additionally, their potential as thermoelectric materials is being explored, particularly for converting waste heat into electricity. Double perovskites are also finding applications in photovoltaics, especially in emerging solar cell technologies, due to their excellent light absorption properties. Overall, the tunable properties of double perovskites make them versatile materials with significant potential in electronics, energy conversion, and environmental applications [10-14].

La-based compounds, such as La<sub>2</sub>BB'O<sub>6</sub> (where B and B' are different transition metals like Cr, Co, or Ni), exhibit half-metallic ferromagnetic properties. These materials are metallic in one spin channel and insulating in the opposite spin channel, making them highly suitable for applications in spintronics and magnetic storage devices. Research has shown that specific compositions, such as La<sub>2</sub>CrCoO<sub>6</sub>, demonstrate exceptional electronic and optical properties, underscoring their potential in optoelectronics as well [15]. Similarly, double perovskites with transition metals, such as La<sub>2</sub>MnMO<sub>6</sub> (where M can be Ni, Co, or Fe), reveal that the magnetic ordering and electronic structure are significantly influenced by the choice of transition metal. For instance, Fe-based compounds tend to exhibit ferrimagnetic behavior, while others may display ferromagnetic properties. These unique characteristics make them promising candidates for energy-efficient magnetic refrigeration technologies [16].

The Bi<sub>2</sub>FeMoO<sub>6</sub> double perovskite is notable for its promising multiferroic properties, exhibiting both ferromagnetic and ferroelectric characteristics, which make it a valuable material for applications

such as spintronic devices. Structurally,  $\text{Bi}_2\text{FeMoO}_6$  adopts a distorted perovskite framework with rhombohedral symmetry. Crystallographic analyses confirm that its structure aligns well with theoretical expectations, displaying lattice parameters that reflect slight deviations from a perfect cubic structure. The unique combination of Fe and Mo in the lattice creates strong Fe–O–Mo superexchange interactions, which drive its magnetic behavior [17]. To understand the detailed changes in the physical properties, we substituted Na and Zn in place of Fe in the host  $\text{Bi}_2\text{FeMoO}_6$ . This study focuses on synthesizing (via solid-state reaction) and characterizing the modified material to explore its potential applications.

## 2. Experimental details

A double perovskite,  $\text{BiNaZnMoO}_6$ , was synthesized using the solid-state reaction method. For the synthesis of this polycrystalline compound, raw materials are;  $\text{Bi}_2\text{O}_3$ ,  $\text{Na}_2\text{CO}_3$ ,  $\text{ZnO}$ , and  $\text{MoO}_2$  of AR grade with 99% purity were procured from LOBA Chemie Pvt. Ltd. The required oxide and carbonate powders were measured stoichiometrically using an electronic digital balance [MODEL: ML 204/A01] with an accuracy of 0.0001 g. The powders were thoroughly mixed using an agate mortar and pestle in dry medium for 3 h, followed by wet mixing for another 3 h. The mixture was then heated at a rate of  $3^\circ\text{C}\cdot\text{min}^{-1}$  for 6 h at  $1050^\circ\text{C}$ . The XRD pattern of the calcined sample was recorded to confirm the formation of a stable crystal structure. Subsequently, polyvinyl alcohol (PVA) was added to the calcined powder to prepare cylindrical pellets with a diameter of 12 mm and a thickness of 2 mm using a KBr hydraulic press under a pressure of  $4.0 \times 10^6 \text{ N}\cdot\text{m}^{-2}$ . The pellets were sintered again in a muffle furnace for 5 h at  $1100^\circ\text{C}$  (heating rate =  $3^\circ\text{C}\cdot\text{min}^{-1}$ ) to remove impurities and increase their density. Structural analysis was performed at room temperature using an X-ray diffractometer [MODEL: Rigaku Ultima IV, source = Cu  $\text{K}\alpha$ , step size =  $0.02^\circ$ ] over a wide range of Bragg's angles ( $20^\circ \leq \theta \leq 80^\circ$ ). To study the distribution and nature of grains (surface microstructure) and their compositional distribution, scanning electron microscopy (SEM) and energy-dispersive X-ray spectroscopy (EDX) analysis, including elemental mapping, were conducted using a ZEISS EVO-18 microscope. For the EDX study, an accelerating voltage of 20 kV and a working distance of approximately 9270  $\mu\text{m}$  were used. High-temperature dielectric data were recorded using an LCR analyzer [MODEL: N4L PSM 1735] over a frequency range of 1 kHz to 1 MHz and a temperature range of  $25^\circ\text{C}$  to  $500^\circ\text{C}$ . In addition to high-temperature studies, the authors also investigated the impedance, capacitance, and dielectric behavior of the sample at low temperatures.

## 3. Results and discussion

### 3.1 XRD analysis

Figure 1(a) represents the XRD pattern at room temperature XRD pattern while Figure 1(b) shows the Gaussian-fitted XRD peak to calculate the scattering angle position and FWHM to find out the average crystallite size using the Scherer's relation.

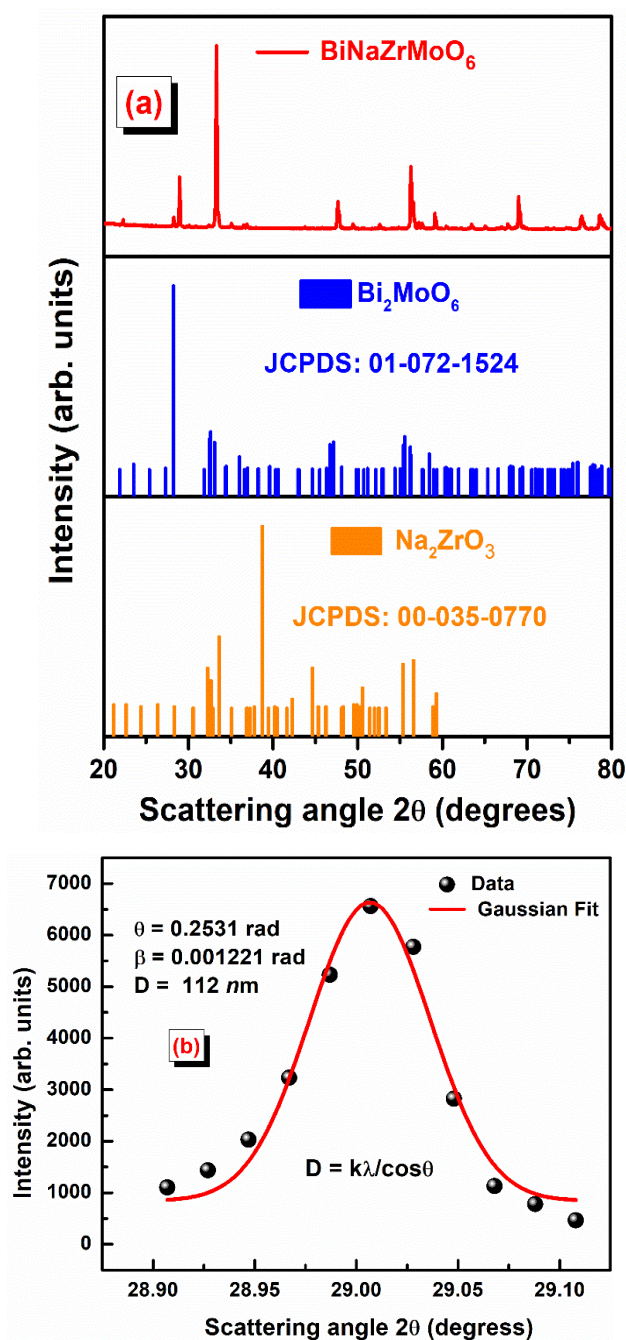


Figure 1. (a) presents the raw XRD data, and (b) the Gaussian fit for peak analysis.

X'Pert HighScore software was used to finalise the structure of the studied sample [18]. For structural analysis of the sample, the X'Pert High-Score Plus software is used. The XRD analysis reveals that the sample has a major phase of orthorhombic crystal symmetry (#  $\text{Bi}_2\text{MoO}_6$ ; JCPDS file No. 01-072-1524) with cell parameters are;  $a = 5.506 \text{ \AA}$ ,  $b = 16.226 \text{ \AA}$ ,  $c = 5.487 \text{ \AA}$ ,  $\alpha = \beta = \gamma = 90^\circ$  volume ( $V$ ) =  $490.21 \text{ \AA}^3$  and density =  $8.26 \text{ g}\cdot\text{cm}^{-3}$  respectively. Again, the sample has a minor phase of monoclinic structure (#  $\text{Na}_2\text{ZrO}_3$ ; JCPDS file No. 00-035-0770) with cell parameters are;  $a = 11.127 \text{ \AA}$ ,  $b = 9.749 \text{ \AA}$ ,  $c = 5.623 \text{ \AA}$ ,  $\alpha = \beta = \gamma = 90^\circ$  volume ( $V$ ) =  $600.77 \text{ \AA}^3$  respectively. Therefore, a solid solution of  $\text{BiNaZnMoO}_6$  double perovskite with a bi-phase structure is formed. Scherer's method is commonly used

to determine the average crystallite size in polycrystalline materials using X-ray diffraction (XRD) data. The general mathematical relation is given by:  $\beta \cos \theta = \frac{k\lambda}{D}$ , where:  $\beta$  is the full-width half maximum (FWHM) in radians,  $\theta$  is the peak position,  $D$  is the average crystallite size,  $k$  is the shape factor for spherical particles (0.89),  $\lambda$  is the X-ray wavelength (1.542 Å) [19]. The average crystallite size ( $D$ ) is found to be 112 nm as shown in Figure 1(b).

### 3.2 Microstructural analysis

Scanning Electron Microscopy (SEM) micrographs are essential for characterizing and visualizing grain size, shape, distribution, and grain boundaries, which are crucial for understanding the relationships between microstructure and the material's electrical properties, as shown in Figure 2(a,b). Additionally, SEM can help in understanding the effects of processing conditions on microstructural development, ultimately guiding the optimization of material synthesis and fabrication methods for specific applications in electronics and energy storage. Furthermore, the average grain size and grain boundaries play pivotal roles in determining the conductivity of polycrystalline materials. In the present study, finer grains can improve conductivity by providing more pathways for charge carriers transport. The ratio of the average grain size to the average crystallite size, i.e., the agglomeration rate, is found to be 6, which may be a strong reason for the elevated dielectric properties [20]. Color mapping is a powerful visualization technique used to analyze the distribution of elements and phases within the material at the microscopic level, as shown in Figure 2(c). By employing scanning electron microscopy (SEM) coupled with EDX analysis, color mapping highlights the presence and concentration of various elements, such as bismuth, sodium, zinc, molybdenum, and oxygen. Each element is represented by a distinct color, allowing researchers to easily identify compositional homogeneity or the presence of secondary phases within the sample.

The energy-dispersive X-ray Spectroscopy (EDX) spectrum of the BNZM ceramic provides essential information regarding its elemental composition and confirms the presence of the intended constituents, as shown in Figure 2(d). In the EDX spectrum, distinct peaks are observed for each element, including bismuth (Bi), sodium (Na), zinc (Zn), molybdenum (Mo), and oxygen (O), with their respective intensities reflecting the stoichiometry of the compound. The relative peak heights allow for quantitative analysis, ensuring that the desired ratios of these elements are achieved during synthesis. Additionally, EDX can identify any impurity phases that may influence the material's properties and performance. In the present study, there are no impurity phases, so better physical properties in the studied sample are expected.

### 3.3 Dielectric analysis

Dielectric studies of ceramic compounds are crucial for understanding their electrical properties and potential applications in advanced electronic devices. These materials often exhibit unique dielectric behavior due to their complex crystal structures and variable composition, making them suitable for applications in capacitors, sensors, and energy storage systems. By investigating dielectric properties such as permittivity,

loss tangent, and relaxation mechanisms, researchers can gain insights into charge transport dynamics, ionic mobility, and phase transitions. This information is essential for optimizing the performance of devices that rely on dielectric materials, such as multilayer capacitors and thermoelectric generators. The degree of polarization affects the material's dielectric constant (permittivity), which quantifies its ability to store electrical energy [21]. Higher polarization generally leads to a higher dielectric constant, enhancing the material's capacity for energy storage in applications such as capacitors. Additionally, polarization impacts the dielectric loss, which refers to the energy dissipated as heat in the material when subjected to an alternating electric field. Understanding the effects of polarization is essential for designing materials with desirable dielectric properties for various electronic and energy storage applications [22].

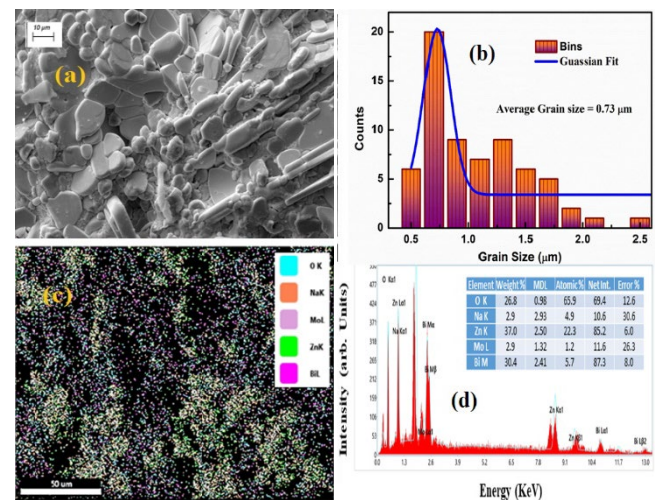


Figure 2. (a, b, c, d) shows the SEM and calculates the average grain size, color mapping, and EDX spectrum of the BNZM ceramic at room temperature.

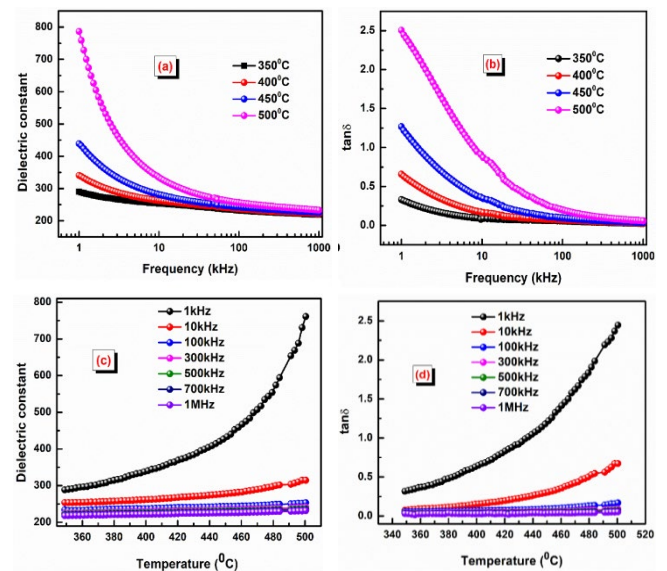


Figure 3. (a, b) shows the dielectric constant versus frequency and  $\tan \delta$  versus frequency of the BNZM ceramic at some selected temperatures, (c, d) shows the dielectric constant versus temperature and  $\tan \delta$  versus temperature of the BNZM ceramic at some selected frequencies.

The effect of frequency on the dielectric constant and dielectric loss in the studied double perovskite compounds is significant and reflects the complex interplay between charge transport mechanisms and polarization processes, as shown in Figure 3(a,b) [25,26]. At low frequencies, the dielectric constant is typically high due to the effective alignment of dipoles and charge carriers, allowing for maximum energy storage. However, as the frequency increases, the dielectric constant often decreases due to the inability of the dipoles to keep pace with the rapidly changing electric field, leading to reduced polarization [24]. Concurrently, the dielectric loss tends to increase at lower frequencies as the material experiences greater energy dissipation from the lagging polarization response. At higher frequencies, the dielectric loss may stabilize or decrease as the charge carriers become less responsive to the alternating field, resulting in lower energy dissipation [25]. Understanding these frequency-dependent behaviors is crucial for optimizing the performance of the studied double perovskite materials in applications such as capacitors, sensors, and energy storage devices, where efficient dielectric properties are essential.

The effect of temperature on the dielectric constant and dielectric loss in the studied double perovskite compounds is a critical aspect of their electrical behavior, as shown in Figure 3(c,d) [26]. As temperature increases, the dielectric constant typically rises due to enhanced ionic mobility and the increased polarization of dipoles within the material. This increased mobility allows for more efficient charge transport and dipole alignment under an applied electric field, resulting in a higher dielectric constant. However, this rise in the dielectric constant is often accompanied by an increase in dielectric loss, particularly at elevated temperatures, as thermal agitation leads to greater energy dissipation from the lagging polarization response [27]. This behavior indicates that while higher temperatures can improve the energy storage capacity of double perovskites, they may also lead to increased losses, which can affect overall efficiency in applications such as capacitors and sensors. Understanding the temperature dependence of these dielectric properties is essential for tailoring the performance of double perovskite materials in various electronic applications [28].

### 3.4 Impedance analysis

The real component of the impedance ( $Z'$ ) of BNZM double perovskite as a function of frequency typically reveals distinctive characteristics indicative of the material's electrical behavior, as shown in Figure 4(a). At low frequencies, the real part of the impedance remains relatively high, reflecting the dominant resistive behavior associated with grain boundary contributions [29]. As the frequency increases, a notable decrease in the real component is observed, suggesting a transition to more capacitive behavior, where the dielectric effects begin to dominate.

This frequency-dependent behavior indicates that charge carriers can respond more effectively to the applied electric field at higher frequencies, highlighting the material's potential for applications in capacitors and other electronic devices. The analysis of the real component versus frequency further emphasizes the significance of BNZM's microstructural properties in influencing its overall electrical performance [30]. The imaginary component of the impedance ( $Z''$ ) of BNZM double perovskite as a function of frequency showcases distinct features that provide insights into the material's dielectric

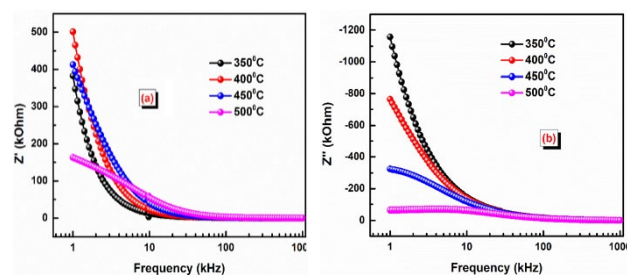


**Figure 4.** (a, b) shows the  $Z'$  versus temperature and  $Z''$  versus frequency of the BNZM ceramic

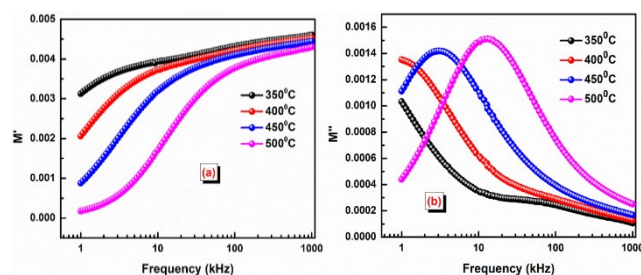


**Figure 5** (a, b) shows  $M'$  versus frequency and  $M''$  versus frequency of the BNZM ceramic.

properties, as shown in Figure 4(b). Typically, the imaginary component exhibits a peak that shifts with varying frequency, indicating the presence of relaxation processes within the material. At low frequencies, the imaginary component tends to be lower, while it increases to a maximum value before decreasing at higher frequencies. This peak is associated with the dielectric relaxation phenomenon, reflecting the response of charge carriers to an alternating electric field. The position of the peak allows for the determination of relaxation time and further elucidates the dynamics of charge transport mechanisms in BNZM [31].

### 3.5 Modulus analysis

The real component of the modulus ( $M'$ ) of BNZM double perovskite as a function of frequency is shown in Figure 5(a). Typically,  $M'$  exhibits a frequency-dependent response, where it increases at low frequencies, reflecting the contribution of ionic and dipolar polarization within the material [32].

As the frequency increases,  $M'$  tends to stabilize and reach a plateau, indicating a saturation of polarization effects. This behavior suggests that at higher frequencies, the charge carriers can no longer respond effectively to the alternating electric field, leading to reduced dielectric losses. The analysis of the real component of the modulus versus frequency highlights the material's potential for applications in capacitors and other electronic devices, where understanding the dielectric response is crucial for optimizing performance [33]. The imaginary component of the modulus ( $M''$ ) of BNZM double perovskite as a function of frequency reveals essential insights into the material's dielectric relaxation dynamics, as shown in Figure 5(b). Typically,  $M''$  exhibits a pronounced peak at specific frequencies, indicating the onset of significant energy dissipation due to the mobility of charge carriers and dipole reorientation within the material. At low frequencies,  $M''$  tends to be relatively low, reflecting minimal energy

loss, while it increases to a maximum value, corresponding to the dominant relaxation processes occurring in the system. As the frequency continues to rise beyond this peak,  $M''$  gradually decreases, signifying that the material's ability to respond effectively to the alternating electric field diminishes [34]. The characteristics of this peak, including its position and height, provide crucial information about the relaxation mechanisms and the overall dielectric behavior of BNZM, underscoring its potential for applications in capacitors and other electronic devices where efficient energy storage and conversion are vital [35].

### 3.6 Cole-Cole and Nyquist's plots

The Nyquist and Cole-Cole plots of BNZM double perovskite provide valuable insights into its dielectric and electrical properties, as shown in Figure 6(a) [inset] and Figure 6(b) respectively. The Cole-Cole plot, representing the complex dielectric constant, shows a semicircular arc, indicating the presence of relaxation processes within the material, which suggests non-Debye-type relaxation behavior [36-38]. The Nyquist plot, typically used for analyzing impedance, displays a depressed semicircular arc, indicating the presence of grain and grain boundary contributions to the electrical conductivity. The arc's size and shape offer information about the resistive and capacitive nature of the material, with BNZM exhibiting semiconducting characteristics, making it suitable for applications in energy storage and electronic devices [39,40].

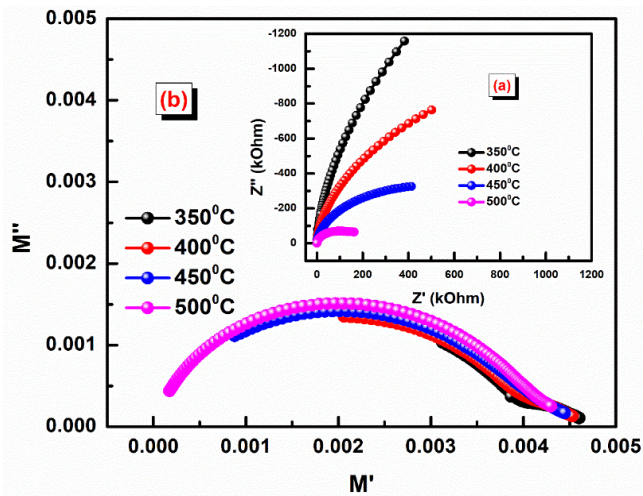


**Figure 6** (a) shows Nyquist's plots [inset], and (b) Cole-Cole's plots of the BNZM ceramic.

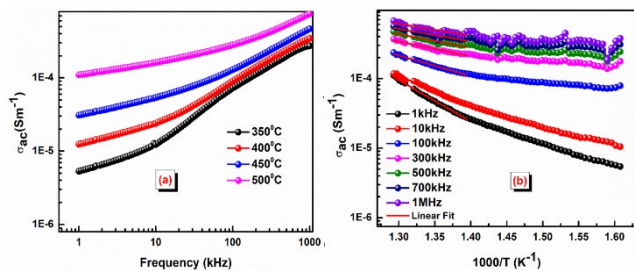


**Figure 7.** (a, b) shows AC conductivity versus frequency and AC conductivity versus temperature of the BNZM ceramic.

### 3.7 AC conductivity study

The AC conductivity of BNZM double perovskite as a function of frequency typically exhibits two distinct regions: a low-frequency plateau and a high-frequency dispersion, as shown in Figure 7(a). At low frequencies, the conductivity remains nearly constant, representing the DC conductivity dominated by long-range charge transport. As the frequency increases, the conductivity shows a power-law dependence, indicating the onset of localized charge carrier hopping between defect sites or ions [41,42]. This frequency-dependent behavior suggests that BNZM follows a hopping conduction mechanism, which is characteristic of many perovskite materials, and points to its potential use in frequency-dependent electronic and dielectric applications, such as capacitors and sensors [43]. The AC conductivity of BNZM double perovskite exhibits a notable dependence on temperature, typically increasing with rising temperature, as shown in Figure 7(b). This behavior indicates enhanced mobility of charge carriers, as thermal energy facilitates the hopping mechanism between localized states. An analysis of the temperature-dependent AC conductivity reveals that it can be described by an Arrhenius-type relationship, allowing for the calculation of the activation energy associated with the conduction process [44].

The activation energy can be calculated using Arrhenius's Equation:

$$\sigma_{ac} = \sigma_0 e^{-\frac{E_a}{k_B T}}$$

where  $E_a$  = activation energy,  $k_B$  = Boltzmann's constant =  $1.38 \times 10^{-23} \text{ J}\cdot\text{K}^{-1}$ . The calculated values of the activation energy are 0.511, 0.384, 0.257, 0.186, 0.167, 0.158, and 0.151 eV at 1, 10, 100, 300, 500, and 700 kHz, and 1 MHz, respectively. The activation energy for BNZM is generally found to be relatively low, suggesting that the charge carriers can move easily, indicating a thermally activated conduction mechanism within the material. This is advantageous for its application in electronic devices [45,46]. The temperature-dependent conductivity further underscores the potential of BNZM for use in applications requiring efficient charge transport across a range of operating conditions.

### 3.8 NTC thermistor

Double perovskite materials, known for their rich variety of structural and electronic properties, have gained attention in the field of Negative Temperature Coefficient (NTC) thermistors. NTC thermistors exhibit a decrease in electrical resistance as temperature increases, making them valuable for temperature sensing and control applications [47-49]. Figure 8(a) shows the variation of resistance versus temperature, while Figure 8(b) represents  $1/T$  versus  $\ln R$  of the BNZM ceramic. As the temperature rises, the thermal energy increases the mobility of charge carriers, such as electrons or oxygen vacancies, leading to enhanced conductivity and, consequently, lower resistance.

This NTC characteristic is particularly notable in BNZM double perovskites with oxygen vacancy-related conduction mechanisms, which provide high sensitivity to temperature changes and may be suitable for temperature sensor devices.

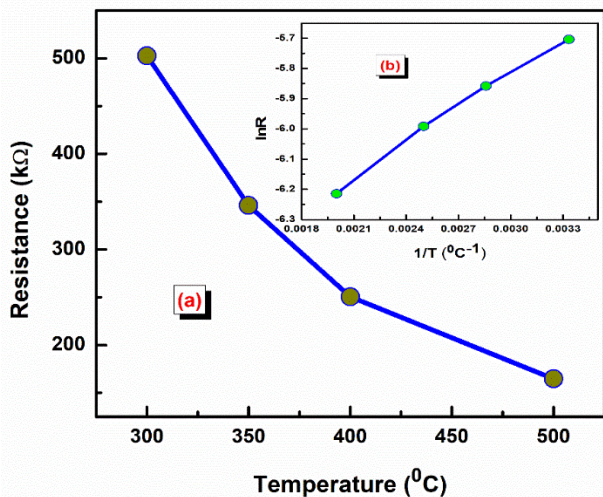


**Figure 8.** (a) shows the resistance versus temperature, and (b) shows the variation of  $\ln R$  versus  $1/T$  of the BNZM ceramic.

Nd, Gd, and La-doped bismuth ferrite ( $\text{BiFeO}_3$ ) shows an interesting behavior called the negative temperature coefficient (NTC) effect, where the material's resistivity drops as the temperature increases. Pratyus Acharya *et al.* studied the effect of the La in the host of  $\text{BiFeO}_3$  and reported different physical properties with possible application [50]. This NTC effect, along with dielectric relaxation, is not unique to this material—it's also seen in other doped bismuth ferrites, like Mn-doped  $\text{BiFeO}_3$ , and in well-known perovskite systems such as  $\text{BaTiO}_3$  and  $\text{SrTiO}_3$ . Scientists often explain these behaviors by pointing to the movement of oxygen vacancies and polaron hopping, which are common in these types of materials. Again, Priyambada Mallick *et al.* studied the structural, dielectric, electrical, and magnetic properties of samarium-doped double perovskite and report the NTC thermistor applications [51]. Again, P. Mallick *et al.* studied the development and characterization of copper-doped perovskite-polymer composite and explore different applications [52]. Meanwhile, research on bismuth ferrite-lithium vanadate ( $\text{BiFeO}_3\text{-LiVO}_3$ ) sheds light on its structural and dielectric properties, with the relaxation behavior being influenced by the presence of lithium vanadate. The material's dielectric loss shows frequency dispersion, a telltale sign of systems where ionic conduction plays a key role and explore the thermistor application [53].

#### 4. Conclusion

The comprehensive study of BNZM double perovskite revealed significant insights into its structural, microstructural, dielectric, and electrical properties. X-ray diffraction confirmed the formation of a mixed phase of orthorhombic and monoclinic solid solution. Microstructural analysis demonstrated a uniform grain distribution with well-defined grain boundaries. The ratio of grain size to average crystallite size is the possible reason for the observed better electrical properties. Dielectric measurements provides a high dielectric constant with low loss, which make the studied sample as a potential candidate for energy storage device applications. The analysis of impedance plots suggests a semiconducting nature, while the study of modulus plots reveals the presence of a non-Debye type relaxation mechanism.

The investigation of AC conductivity indicates the occurrence of a thermally activated conduction mechanism. Additionally, the study of resistance versus temperature further supports the semiconducting nature of the sample. These findings highlight its viability as a candidate for advanced functional materials in electronic energy storage devices and NTC thermistor applications.

#### Acknowledgements

The authors would like to express their sincere gratitude to the host Institution for providing the XRD and SEM-EDX characterization.

#### References

- [1] S.-S. Rong, M. B. Faheem, and Y.-B. Li, "Perovskite single crystals: Synthesis, properties, and applications," *Journal of Electronic Science and Technology*, vol. 19, p. 100081, 2021.
- [2] N. K. Elangovan, R. Kannadasan, B. B. Beenarani, M. H. Alsharif, M.-K. Kim, and Z. H. Inamul, "Recent developments in perovskite materials, fabrication techniques, band gap engineering, and the stability of perovskite solar cells," *Energy Reports*, vol. 11, pp. 1171-1190, 2024.
- [3] W. Li, Z.-M. Wang, F. Deschler, S. Gao, R. H. Friend, and A. K. Cheetham, "Chemically diverse and multifunctional hybrid organic-inorganic perovskites," *Nature Reviews Materials*, vol. 2, p. 16099, 2017.
- [4] N. H. Tiep, Z.-L. Ku, and H.-J. Fan, "Recent advances in improving the stability of perovskite solar cells," *Advanced Energy Materials*, vol. 6, p. 1501420, pp. 1-19, 2016.
- [5] N. J. Jeon, J. H. Noh, W.-S. Yang, Y. C. Kim, S. Ryu, J. Seo, and S. I. Seok, "Compositional engineering of perovskite materials for high-performance solar cells," *Nature*, vol. 517, pp. 476-480, 2015.
- [6] S. D. Stranks, G. E. Eperon, G. Grancini, C. Menelaou, M. J. P. Alcocer, T. Leijtens, L. M. Herz, A. Petrozza, and H. J. Snaith, "Electron-hole diffusion lengths exceeding 1 micrometer in an organometal trihalide perovskite absorber," *Science*, vol. 342, pp. 341-344, 2013.
- [7] N. Suresh Kumar, and K. Chandra Babu Naidu, "A review on perovskite solar cells (PSCs), materials and applications," *Journal of Materiomics*, vol. 7, pp. 940-956, 2021.
- [8] B. Niu, F. Jin, L. Zhang, P. Shen, and T. He, "Performance of double perovskite symmetrical electrode materials  $\text{Sr}_2\text{TiFe}_{1-x}\text{Mo}_x\text{O}_{6-\delta}$  ( $x=0.1,0.2$ ) for solid oxide fuel cells," *Electrochimica Acta*, vol. 263, pp. 217-227, 2018.
- [9] Q. Sun, Z. Dai, Z. Zhang, Z. Chen, H. Lin, Y. Gao, and D. Chen, "Double perovskite  $\text{PrBaCo}_2\text{O}_{5.5}$ : An efficient and stable electrocatalyst for hydrogen evolution reaction," *Journal of Power Sources*, vol. 427, pp. 194-200, 2019.
- [10] S. S. Nair, L. Krishnia, A. Trukhanov, P. Thakur, and A. Thakur, "Prospect of double perovskite over conventional perovskite in photovoltaic applications," *Ceramics International*, vol. 48, pp. 34128-34147, 2022.
- [11] H. Lin, P. Liu, S. Wang, Z. Zhang, Z. Dai, S. Tan, and D. Chen, "A highly efficient electrocatalyst for oxygen reduction reaction:

- Three-dimensionally ordered macroporous perovskite LaMnO<sub>3</sub>," *Journal of Power Sources*, vol. 412, pp. 701-709, 2019.
- [12] S. Dixit, "Solar technologies and their implementations: A review," *Materials Today: Proceedings*, vol. 28, pp. 2137-2148, 2020.
- [13] G.-H. Kim, and D. S. Kim, "Development of perovskite solar cells with >25% conversion efficiency," *Joule*, vol. 5, pp. 1033-1035, 2021.
- [14] P. A. Jebakumar, D. J. Moni, D. Gracia, and M. D. Shallet, "Design and simulation of inorganic perovskite solar cell," *Applied Nanoscience*, vol. 12, pp. 1507-1518, 2022.
- [15] M. U. Rehman, Q. Wang, and Y. Yu, "Electronic, magnetic and optical properties of double perovskite compounds: A first principle approach," *Crystals*, vol. 12, p. 1597, 2022
- [16] R. Das, S. Bhattacharya, A. Haque, D. Ghosh, O. I. Lebedev, A. Gayen, and M. M. Seikh, "A comparative magnetic behavior of conventional and high entropy double perovskites: La<sub>2</sub>MnCoO<sub>6</sub> and (La<sub>0.4</sub>Y<sub>0.4</sub>Ca<sub>0.4</sub>Sr<sub>0.4</sub>Ba<sub>0.4</sub>)MnCoO<sub>6</sub>," *Journal of Magnetism and Magnetic Materials*, vol. 538, p. 168267, 2021.
- [17] Z. Pei, K. Leng, W. Xia, Y. Lu, H. Wu, and X. Zhu, "Structural characterization, dielectric, magnetic and optical properties of double perovskite Bi<sub>2</sub>FeMnO<sub>6</sub> ceramics," *Journal of Magnetism and Magnetic Materials*, vol. 508, p. 166891, 2020.
- [18] S. Mishra, R. N. P. Choudhary, and S. K. Parida, "Structural, dielectric, electrical and optical properties of Li/Fe modified barium tungstate double perovskite for electronic devices," *Ceramics International*, vol. 48, pp. 17020-17033, 2022.
- [19] B. D. Cullity, and R. S. Stock, *Elements of X-Ray Diffraction.*, New Jersey: Prentice-Hall, 2001.
- [20] A. B. J. Kharrat, N. Moutia, K. Khirouni, and W. Boujelben, "Investigation of electrical behavior and dielectric properties in polycrystalline Pr<sub>0.8</sub>Sr<sub>0.2</sub>MnO<sub>3</sub> manganite perovskite," *Materials Research Bulletin*, vol. 105, pp. 75-83, 2018.
- [21] H. P. P. V. Shanmugasundram, E. Jayamani, and K. H. Soon, "A comprehensive review on dielectric composites: Classification of dielectric composites," *Renewable and Sustainable Energy Reviews*, vol. 157, p. 112075, 2022.
- [22] M. M. Salem, L. V. Panina, E. L. Trukhanova, M. A. Darwish, A. T. Morchenko, T. I. Zubar, S. V. Trukhanov, and A. V. Trukhanov, "Structural, electric and magnetic properties of (BaFe<sub>11.9</sub>A<sub>0.1</sub>O<sub>19</sub>)<sub>1-x</sub> - (BaTiO<sub>3</sub>)<sub>x</sub> composites," *Composites Part B: Engineering*, vol. 174, p. 107054, 2019.
- [23] V. Koval, G. Viola, M. Zhang, M. Faberova, R. Bures, and H. Yan, "Dielectric relaxation and conductivity phenomena in ferroelectric ceramics at high temperatures," *Journal of the European Ceramic Society*, vol. 44, pp. 2886-2902, 2024
- [24] J. R. Macdonald, "Theory of space-charge polarization and electrode-discharge effects," *The Journal of Chemical Physics*, vol. 58, no. 11, pp. 4982-5001, 1973.
- [25] M. Maglione, "Free charge localization and effective dielectric permittivity in oxides," *Journal of Advanced Dielectrics*, vol. 6, p. 1630006, 2016
- [26] N. Hirose, and A. R. West, "Impedance spectroscopy of undoped BaTiO<sub>3</sub> ceramics," *Journal of the American Ceramic Society*, vol. 79, pp. 1633-1641, 1996.
- [27] S. Mishra, R. N. P. Choudhary, and S. K. Parida, "A novel double perovskite BaKFeWO<sub>6</sub>: Structural, microstructural, dielectric and optical properties," *Inorganic Chemistry Communications*, vol. 145, p. 110068, 2022.
- [28] K. S. Cole, and R. H. Cole, "Dispersion and absorption in dielectrics I. Alternating current characteristics," *The Journal of Chemical Physics*, vol. 9, pp. 341-351, 1941.
- [29] J. T. Irvine, D. C. Sinclair, and A. R. West, "Electroceramics: characterization by impedance spectroscopy," *Advanced Materials*, vol. 2, pp. 132-138, 1990.
- [30] S. Mishra, S.K. Parida, "Electrical and optical properties of a lead-free complex double perovskite BaNaFeMoO<sub>6</sub>: Photovoltaic and thermistor applications," *Materials Science and Engineering: B*, vol. 296, pp. 116629-116645, 2023
- [31] X. Guo, Z. Zhang, W. Sigle, E. Wachsman, and R. Waser, "Schottky barrier formed by a network of screw dislocations in SrTiO<sub>3</sub>," *Applied Physics Letters*, vol. 87, p. 162105, 2005
- [32] S. K. Parida, S. Moharana, S. Sagadevan, "A double perovskite BaSrTiMnO<sub>6</sub>: Synthesis, microstructural, transport and optical properties for NTC thermistor applications," *Journal of Molecular Structure*, vol. 1316, pp. 138925, 2024
- [33] B. Tilak, "Ferroelectric relaxor behavior and spectroscopic properties of Ba<sup>2+</sup> and Zr<sup>4+</sup> modified sodium bismuth titanate," *American Journal of Materials Science*, vol. 2, pp. 110-118, 2012.
- [34] K. Kumari, A. Prasad, and K. Prasad, "Dielectric, impedance/modulus, and conductivity studies on [Bi<sub>0.5</sub>(Na<sub>1-x</sub>K<sub>x</sub>)<sub>0.5</sub>] 0.94Ba<sub>0.06</sub>TiO<sub>3</sub> (0.16 ≤ x ≤ 0.20) lead-free ceramics," *American Journal of Materials Science*, vol. 6, pp. 1-18, 2016.
- [35] K. Kumari, A. Prasad, and K. Prasad, "Dielectric, impedance/modulus, and conductivity studies on [Bi<sub>0.5</sub>(Na<sub>1-x</sub>K<sub>x</sub>)<sub>0.5</sub>] 0.94Ba<sub>0.06</sub>TiO<sub>3</sub> (0.16 ≤ x ≤ 0.20) lead-free ceramics," *American Journal of Materials Science*, vol. 6, pp. 1-18, 2016.
- [36] A. K. Jonscher, "Dielectric relaxation in solids," *Journal of Physics D: Applied Physics*, vol. 32, pp. R57-R70, 1999.
- [37] A. Goswami, and P. K. Mahapatra, "Impedance spectroscopy and Cole-Cole analysis of dielectric properties in lead-based ceramic materials," *Ceramics International*, vol. 40, pp. 7291-7300, 2014.
- [38] R. K. Upadhyay, and R. Kumar, "Analysis of Cole-Cole impedance plots of dielectric ceramics using complex impedance spectroscopy," *Materials Science and Engineering: B*, vol. 177, pp. 923-929, 2012
- [39] R. Kumar, and S. B. Rai, "Electrical and dielectric properties of ferrite ceramics through nyquist plot interpretation," *Journal of Materials Science: Materials in Electronics*, vol. 28, pp. 7893-7900, 2017.
- [40] W. Song, and Y. H. Lee, "Nyquist plot analysis of electrical properties in perovskite-based ceramics," *Solid State Ionics*, vol. 181, pp. 1658-1664, 2010.
- [41] S. Ghosh, and T. P. Sinha, "AC Conductivity and dielectric relaxation in perovskite oxides: Frequency and temperature analysis," *Journal of Applied Physics*, vol. 98, p. 074109, 2005.
- [42] A. Kumar, and R. Prakash, "Temperature and frequency dependence of AC conductivity in ferrite ceramics," *Journal*

- of *Materials Science: Materials in Electronics*, vol. 23, pp. 940-947, 2012.
- [43] P. Lunkenheimer, and A. Loidl, "AC conductivity studies on relaxor ferroelectric ceramics: Frequency and temperature dependence," *Physical Review B*, vol. 67, no. 5, p. 052102, 2003.
- [44] B. V. R. Chowdari, and L. Guo, "AC conductivity and dielectric properties of perovskite ceramics at various temperatures," *Solid State Ionics*, vol. 86-88, pp. 1007-1012, 1996.
- [45] H. S. Nagaraja, and R. V. Anavekar, "Frequency and temperature dependence of AC conductivity in MgO-based ceramic compounds," *Materials Science and Engineering: B*, vol. 140, pp. 20-25, 2007.
- [46] D. C. Sinclair, and A. R. West, "Impedance and modulus spectroscopy of semiconducting BaTiO<sub>3</sub> showing positive temperature coefficient of resistance," *Journal of Applied Physics*, vol. 66, pp. 3850-3856, 1989.
- [47] A. Feteira, "Negative temperature coefficient resistance (NTCR) ceramic thermistors: An industrial perspective," *Journal of the American Ceramic Society*, vol. 92, pp. 967-983, 2009.
- [48] Y. Saad, I. Álvarez-Serrano, M. L. López, and M. Hidouri, "Dielectric response and thermistor behavior of lead-free x NaNbO<sub>3</sub>-(1-x) BiFeO<sub>3</sub> electroceramics," *Ceramics International*, vol. 44, pp. 18560-18570, 2018.
- [49] S. Sahoo, "Enhanced time response and temperature sensing behavior of thermistor using Zn-doped CaTiO<sub>3</sub> nano-particles," *Journal of Advanced Ceramics*, vol. 7, pp. 99-108, 2018.
- [50] P. Acharya, R. N. P. Choudhary, and S. K. Parida, "Effect of lanthanum on structural, dielectric, electrical, and optical properties of the bismuth ferrite," *Brazilian Journal of Physics*, vol. 54, pp. 1-18, 2024.
- [51] P. Mallick, S. K. Satpathy, and B. Behera, "Study of structural, dielectric, electrical, and magnetic properties of samarium-doped double perovskite material for thermistor applications," *Brazilian Journal of Physics*, vol. 52, pp. 187-201, 2022.
- [52] P. Mallick, R. Patra, D. Mohanty, and S. K. Satpathy, "Development and characterization of copper-doped perovskite-polymer composite through high-temperature technique," *Sādhanā*, vol. 47, pp. 134-140, 2022.
- [53] M. K. Sahu, P. Mallick, S. K. Satpathy, and B. Behera, "Structural, dielectric, and electrical study of bismuth ferrite-lithium vanadate," *The European Physical Journal Applied Physics*, vol. 97, pp. 72-78, 2022.